Large Apparent Electric Size of Solid-State Nanopores Due to Spatially Extended Surface Conduction

ARTICLE *in* NANO LETTERS · JULY 2012

Impact Factor: 13.59 · DOI: 10.1021/nl301412b · Source: PubMed

6 AUTHORS, INCLUDING:

Choongyeop Lee
Kyung Hee University
18 PUBLICATIONS **441** CITATIONS
SEE PROFILE

Laurent Joly
Claude Bernard University Lyon 1
39 PUBLICATIONS **841** CITATIONS
SEE PROFILE

Remy Fulcrand
French National Centre for Scientific Research
22 PUBLICATIONS **238** CITATIONS
SEE PROFILE

Lyderic Bocquet
Ecole Normale Supérieure de Paris
174 PUBLICATIONS **7,429** CITATIONS
SEE PROFILE

NANO LETTERS

Letter

pubs.acs.org/NanoLett

Large Apparent Electric Size of Solid-State Nanopores Due to Spatially Extended Surface Conduction

Choongyeop Lee, Laurent Joly, Alessandro Siria, Anne-Laure Biance, Rémy Fulcrand, and Lydéric Bocquet*

LPMCN, Université de Lyon; UMR 5586 Université Lyon 1 et CNRS, F-69622 Villeurbanne, France

ABSTRACT: Ion transport through nanopores drilled in thin membranes is central to numerous applications, including biosensing and ion selective membranes. This paper reports experiments, numerical calculations, and theoretical predictions demonstrating an unexpectedly large ionic conduction in solid-state nanopores, taking its origin in anomalous entrance effects. In contrast to naive expectations based on analogies with electric circuits, the surface conductance inside the nanopore is shown to perturb the three-dimensional electric current streamlines far outside the nanopore in order to meet charge conservation at the pore entrance. This unexpected contribution to the ionic conductance can be interpreted in terms of an apparent electric size of the solid-state nanopore, which is much larger than its geometric counterpart whenever the number of charges carried by the nanopore surface exceeds its bulk counterpart. This apparent electric size, which can reach hundreds of nanometers, can have a major impact on the electrical detection of translocation events through nanopores, as well as for ionic transport in biological nanopores.

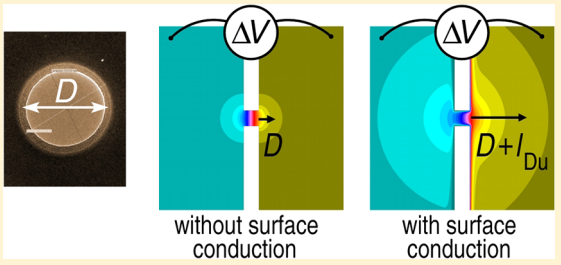

KEYWORDS: *Nanofluidics, nanopore, ion transport, surface conduction, entrance effects*

Nanopores have received a lot of attention in recent years[1] for their potential applications as low-cost, high-throughput biosensors,[2,3] and membranes for filtering,[4,5] desalination,[6] and energy generation.[7] Short transit length for ions or biomolecules and nanometric detection area in a nanopore are advantageous for biosensing in terms of spatial resolution and sensitivity. It has been demonstrated that translocation of nanoparticles[8] or biomolecules such as DNA,[9] proteins,[10] and viruses[11] through a nanopore can be detected by monitoring the ionic current across this pore. A partial blockage of a pore by a target object leads to a transient downward pulse of ionic current, the magnitude and duration of which is directly related to physical properties of the target (e.g., diameter and length) or its interaction with the pore surface. This is expected to translate into the necessary information for DNA sequencing,[12] protein detection,[10] and nanoparticle-based immunoassay.[13] A signature in ion current is used for sensing, and thus an understanding of ion current in a nanopore, for example, how surface effects and bulk effects contribute to the ion current, is required in designing nanopore-based biosensors. In a different context, new perspectives on ion transport through nanopores have been suggested in an effort to engineer smart membranes for filtering, desalination, and energy generation.[6,7,14]

The present paper describes an experimental investigation of ion transport through solid-state nanopores as a function of pore size and ionic strength. An unexpectedly large conductance at small and moderate ion concentrations is demonstrated, which is in contrast to simple expectations based on analogies with equivalent electric circuits. Using full numerical calculations of ion transport in the nanopore, we show that this effect stems from three-dimensional entrance effects outside the pore that couple to surface conduction inside the pore. This unforeseen coupling, which occurs so as to maintain charge conservation at the pore entrance,[15] does strongly perturb the electric current streamlines outside the pore and maintains a high conductance path even at low ion concentration. This effect is rationalized on the basis of an analytical model for ion conduction, which reproduces both numerical and experimental results. As a result, ion conduction through the nanopore is characterized by an apparent electric size that is much larger than its bare geometric diameter whenever the salt concentration is small and/or the surface charge on the pore surface is large, reaching hundreds of nanometers in these conditions. Accordingly, the electrical resistance of the pore does not depend on its diameter anymore in this regime: tiny pores conduct as well as much larger pores.

Entrance Effects and Ion Conduction. A nanopore differs from a nanochannel in that its length is comparable to or smaller than its diameter, and is thus defined by a rather small aspect ratio. Recently, ion transport in nanochannels with a channel length much larger than the channel height or diameter has been exhaustively investigated as a function of size and ionic strength, see, for example, refs 16 and 17, and a good understanding has now emerged. Altogether ion conduction was shown to be a combination of bulk and surface

Received: April 15, 2012
Revised: June 29, 2012
Published: July 2, 2012

   dx.doi.org/10.1021/nl301412b | *Nano Lett.* 2012, 12, 4037−4044

contributions; while bulk conduction is attributed to ions inside the bulk of the pore, surface conduction arises due to excess counterions close to the surface screening the surface charge, the so-called electric double layer (EDL).[17,18] Accordingly, at high salt concentration the ion conduction is mainly determined by the bulk conductivity, κ_b, but at low salt concentration, the surface conduction, determined by the surface conductivity κ_s, becomes dominant over the bulk conduction, leading to a saturation of the measured ion conductance. This crossover occurs for nanochannel cross sizes lower than the so-called Dukhin length, defined as the surface to bulk conductivity ratio, $l_{Du} = \kappa_s/\kappa_b$.[15,18] In contrast, ion transport in nanopores pierced in thin membranes is paradoxically far more complex than in nanochannels; due a much smaller aspect ratio, ion transport cannot be reduced to a one-dimensional view as for a nanochannel, and the three-dimensional nature of a nanopore makes it difficult to comprehend ion transport in a nanopore on the basis of simple electric analogies. Although the access effect was often neglected in interpreting ion conductance in a nanopore,[19,20] it has been long known (in particular in the physiology literature[21,22]) that the entrance imparts additional resistance against ion transport, commonly referred to as access resistance,[23] and results in a lower conductance.[21,22,24,25] Several approximated forms were proposed in an attempt to account for the complex three-dimensional (3D) entrance geometry of the pore. For example, Hall[22] suggested that the access resistance of a pore could be accounted for by considering a semispherical cupola as an effective electrode,[22,25] leading to a nanopore conductance behaving as

$$G_0 = \kappa_b\left[\frac{4L}{\pi D^2} + \frac{1}{D}\right]^{-1} \quad (1)$$

where the second term accounts for the entrance effect; κ_b is the bulk conductivity, L and D are the length and diameter of the nanopore, respectively. This result assumes that the resistance of the nanopore is the sum of the resistance inside the pore, plus the entrance resistance that behaves typically like $(D\kappa_b)^{-1}$. This expression was recently further generalized to more realistic hourglass-shaped pores.[25] An interesting prediction of this expression is that for nanopores, associated with small aspect ratio $L/D < 1$, the conductance scales merely like the diameter $G_0 \propto D$, while for long nanochannels with $L \gg D$ one expects a much stronger dependence, scaling as $G_0 \propto D^2$. Entrance effects have accordingly a strong impact on nanopores conductance.

The access resistance has received more attention in recent years, as nanopores pierced in ultrathin membrane, like graphene, emerged as a new class of nanopore with enhanced performance.[26−28] On the other hand, there have been few studies as to how surface effects contribute to the conductance in a nanopore.[19,20] We show here that the 3D nature of the nanopore opens a new conductance path that plays a key role for the conductance at low ionic concentration.

Nanopores and Conductance Experiments. We fabricated nanopores by drilling silicon nitride (SiN) membranes, 100 nm in thickness, with pore diameters D in the range 140, 160, 250, 430, and 520 nm. The largest pores (D = 250, 430, and 520 nm) had a cylindrical shape, but nanopores with D = 140 and 160 nm were slightly conical (±10 nm in diameter). The ion conductance through the nanopore was measured in a home-built flow cell with the pierced membrane separating two fluidic reservoirs (Figure 1). Potassium chloride solutions with concentration varying between 5×10^{-5} and 1 M (mol/L) were

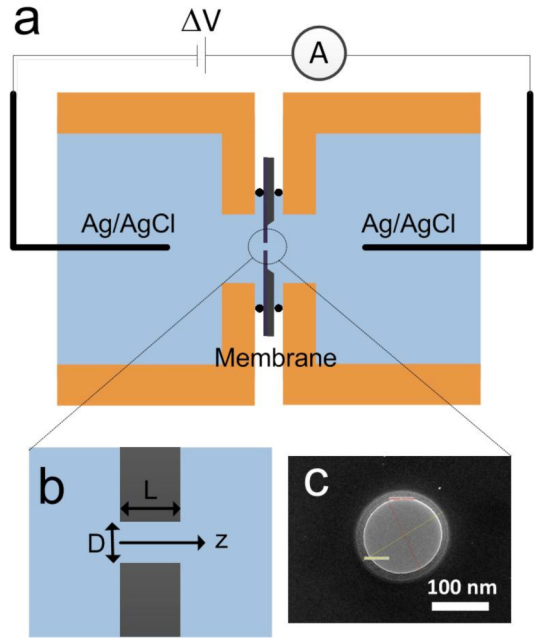

Figure 1. (a) Schematic of a flow cell and (b) sketch of cross-section of a nanopore. (c) Transmission electron microscopy image of a nanopore with 140 nm diameter.

considered (with fixed pH 6) and the voltage was imposed using Ag/AgCl electrodes (see Methods for details). For all experimental data points, the salt concentration c_s was obtained from independent bulk conductivity measurements.

The experimental data for the measured conductance are shown in Figure 2a for a wide range of salt concentrations and

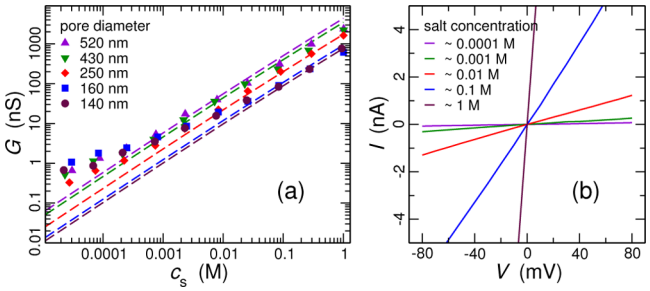

Figure 2. (a) Measured conductance over varying salt concentration in nanopores with different diameters. As a comparison, the predicted conductance from eq 1 is plotted together as dashed lines. The deviation between the experimental data and the prediction of eq 1 becomes larger at low salt concentration, where the latter strongly underestimates the conductance. (b) Current−voltage curves in a nanopore with 140 nm diameter.

various nanopore sizes. A representative set of voltage-current curves for 140 nm diameter nanopore is shown in Figure 2b. An interesting feature of these results is that the conductance depends markedly on the pore diameter for large salt concentration but appears to converge to a similar value for low salt concentration. The predicted conductance accounting for the geometric access effect in eq 1, using the bulk conductivity κ_b measured independently, is plotted in Figure 2

dx.doi.org/10.1021/nl301412b | Nano Lett. 2012, 12, 4037−4044

as a comparison with experimental data. At high salt concentration, experimental results are in good agreement with the prediction, in line with previous experimental studies.[25,26] In particular the dependence of the conductance on diameter is indeed found to be weaker than the prediction in the absence of entrance effects (for which $G \propto D^2$). Corrections due to entrance effects are essential to account for the experimental data. However, at salt concentrations lower than $\sim 10^{-2} - 10^{-3}$ M, deviation from the predicted conductance becomes apparent and eq 1 underestimates the measured conductance by up to 1 order of magnitude.

As a first approach, one may discuss this observation in terms of the characteristic length scales of the problem. First, one may immediately realize that such effects cannot originate in the overlap of EDLs inside the nanopore, as suggested in a previous work using much smaller pores.[19] The expression of the Debye length, the characteristic thickness of the EDL, is given by $\lambda_D = [(\varepsilon k_B T)/(2e^2 c_s)]^{1/2}$ where c_s is the salt concentration, ε is the dielectric permittivity of water, k_B is the Boltzmann constant, $T \sim 300$ K is the absolute temperature, and e is the elementary charge.[17,18] At 1 mM KCl concentration, where a strong deviation from the bulk prediction is observed in Figure 2, one has $\lambda_D \simeq 10$ nm, still far below the typical size of the pore. Alternatively, and in analogy with similar observations for nanochannels, the above results could point to surface conduction effects. The latter is characterized by the so-called Dukhin length introduced above

$$l_{Du} = \frac{\kappa_s}{\kappa_b} \tag{2}$$

where κ_s is the surface conductivity and κ_b is the bulk conductivity. This length accounts for the relative importance of the surface conduction in the pore as compared to the bulk conduction.[18] Using a Poisson−Boltzmann estimate for κ_s (see ref 18 and Methods), one may rewrite this length as $l_{Du} \approx (|\Sigma|/e)/(2c_s)$, where Σ is the surface charge density and c_s is the bulk salt concentration. With a surface charge $|\Sigma| = 20$ mC/m^2, a typical value for a silicon nitride surface,[19,29,30] the Dukhin length is expected to be 100 nm at 1 mM KCl. This order of magnitude for the Dukhin length compares directly with the diameter of the pore, thereby showing that the surface conduction mechanism should be indeed relevant for the phenomena under scrutiny.

This leads to the central question on how to associate surface conduction with access effects in thin pores. In strong contrast to long nanochannels, entrance contributions cannot be omitted for pores due to their small aspect ratio L/D, as, for example, highlighted in eq 1, and a proper description should combine both effects of surface conduction in the pore and entrance contributions outside of the pore.

As a first attempt, one may try to extend the approach proposed by Hille and Hall[21,22] in order to account for the surface conduction inside the nanopore together with entrance effects. The descriptions for entrance effects are based on the idea that the pore can be considered as several resistances in series[21,22] with the resistance inside the pore R_p supplemented by the access resistances R_{out} on each side of the pore: $R = R_p + 2R_{out}$, so that the overall conductance verifies $G = (G_p^{-1} + 2G_{out}^{-1})^{-1}$.

Following Hall and Hille,[21,22] the access conductance can be written as $G_{out} = \alpha \kappa_b D$, where α is a geometrical prefactor that depends on the model used (e.g., $\alpha = 2$ in Hall[22]). In terms of scaling, the physical idea behind this result is that the amplitude of the electric field outside of the pore is mainly fixed by the voltage drop, ΔV_{out}, divided by a typical scale fixed by the diameter D of the pore, $E_{out} \sim \Delta V_{out}/D$ and not the (macroscopic) distance between the electrodes. The current I writes accordingly: $I \sim (\kappa_b D^2)(\Delta V_{out}/D)$. A more proper estimation proposed by Hall[22] can be made by considering the full 3D calculation of an equivalent electrostatic problem with a geometry given by an electrode at infinity and an equipotential in a disk accounting for the entrance of the pore.

Now, in the classic approaches by Hille and Hall,[21,22] the pore electric conductance G_p is usually assumed to be proportional to the bulk conductivity $G_p = \kappa_b[(\pi D^2)/(4L)]$. As a first approach, one may thus simply add the contribution of the surface conduction in this expression with

$$G_p = \kappa_b \frac{\pi D^2}{4L} + \kappa_s \frac{\pi D}{L} \tag{3}$$

This leads to the following expression for the overall conductance

$$G = \kappa_b \left[\frac{4L}{\pi D^2} \frac{1}{1 + 4\frac{l_{Du}}{D}} + \frac{2}{\alpha D} \right]^{-1} \tag{4}$$

Note that this naturally introduces the Dukhin number $Du = 4\kappa_s/(\kappa_b D) = 4l_{Du}/D$, which can be defined as the ratio between the surface and bulk contributions to the electric current inside the pore.

This expression in eq 4 extends the classical expression for the conductance with surface contributions in eq 3[16,20] in order to account for finite aspect ratio L/D of the channel.

The above expression for the conductance predicts a crossover between two regimes. Using $\kappa_b \propto c_s$, then $Du \propto c_s^{-1} \to 0$ at large salt concentration and one recovers the classic expression for the conductance accounting for entrance effects $G \simeq G_0$, as defined in eq 1. It is indeed linear in salt concentration. However, at low salt concentration with $Du \to \infty$, the conductance scales as $G \simeq \kappa_b[(\alpha D)/2]$, again linear in concentration. Accordingly, no saturation of the conductance is predicted at low salt concentration from this first approach, which is in contrast to what occurs for infinitely long pores, corresponding to $L \gg D$ in eq 4. Physically, this is because the conductance outside of the pore, G_{out}, vanishes for low salt concentration, thereby limiting the global electric conductance. Note that assuming a surface charge that depends on salt concentration, as proposed, for example, in ref 20, does not modify this conclusion, as the surface conduction κ_s becomes irrelevant in this regime. In any case, access effects are predominant for vanishing salt concentration because the corresponding access resistance R_{out} becomes infinite in this limit.

Therefore, this approach fails to reproduce the experimental results in Figure 2, which exhibit a saturation of the conductance at low salt concentration.

Altogether the observation of a large conduction in a nanopore at small concentration points to a more complex scenario than in nanochannels. As we will show below, the understanding of this effect requires to fully revisit the 3D conduction paths inside and outside the nanopore and points to an unforeseen conduction mechanism.

Numerical Calculations of Conductance Inside a Nanopore. In order to get further insights into the ion transport mechanisms inside a nanopore, we performed

dx.doi.org/10.1021/nl301412b | Nano Lett. 2012, 12, 4037−4044

exhaustive numerical calculations of ion transport through a small aperture. To this end, we solved the Poisson–Nernst–Planck equations for the electric potential V and the K^+/Cl^- ion concentration $c_\pm$ using finite-element method (COMSOL). The corresponding equations coupling the electric potential V to the ion concentrations $c_\pm$ write

$$\nabla\cdot(-\varepsilon\nabla V) = e(c_+ - c_-); \qquad \nabla\cdot\boldsymbol{N}_\pm = 0 \tag{5}$$

where ε is the water permittivity, e the elementary charge, and $\boldsymbol{N}_\pm$ are the K^+/Cl^- fluxes:

$$\boldsymbol{N}_\pm = -\mu k_B T\nabla c_\pm \mp e\mu c_\pm \nabla V \tag{6}$$

with μ the ion mobility (assumed to be equal for K^+ and Cl^-).

We considered a pore of diameter D and length L using a 2D axisymetric geometry presented in Figure 3. We imposed the

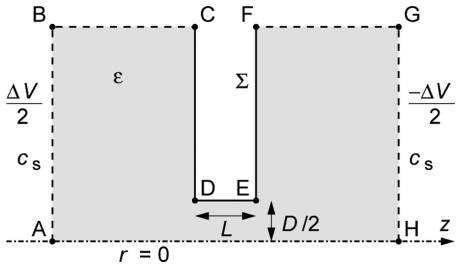

Figure 3. Axisymetric geometry of the pore with diameter D and length L used for the numerical resolution of the Poisson–Nernst–Planck equations using a finite-element solver (COMSOL). (CDEF) represents the membrane boundaries; the electric potential drop is imposed between equipotentials (AB) and (GH).

following boundary conditions. The membrane (CDEF in Figure 3) carried a surface charge Σ, $\boldsymbol{n}\cdot(-\varepsilon\nabla V) = \Sigma$, and was impermeable to ions, $\boldsymbol{n}\cdot\boldsymbol{N}_\pm = 0$. Far from the pore in the radial direction (BC–FG), we imposed a symmetry condition, $n\cdot(-\varepsilon\nabla V) = 0$; $\boldsymbol{n}\cdot\boldsymbol{N}_\pm = 0$. Also, we required that both ion concentrations relaxed toward the bulk salt concentration far from the pore in the axial direction (AB–GH), $c_\pm = c_s$, and we imposed a potential difference between the two reservoirs, $V = \Delta V/2$ on AB and $V = -\Delta V/2$ on GH. In order to limit finite size effects, we imposed that the size of the reservoirs was much larger than the pore diameter, the Debye length, and the Dukhin length. Furthermore, in order to correctly describe the EDLs, we also took care that the mesh size was smaller than the Debye (λ_D) and Gouy–Chapman ($l_{GC} \propto |\Sigma|^{-1}$, see ref 18 and Methods) lengths close to the charged walls. Consequently, the range of surface charges and concentrations accessible was limited because the ratio l_{Du}/l_{GC} could not be too large. The conductance G is given by the electric current across the pore (integral of the electric flux $e(\boldsymbol{N}_+ - \boldsymbol{N}_-)$ over any cross-section of the system) divided by the imposed potential difference.

Figure 4 shows the predicted conductance as a function of the salt concentration and pore diameter. Altogether the numerical results do fully reproduce the experimental observations: ion conductance in nanopores strongly departs from bulk behavior in the low concentration regime, showing a saturation and a weak dependence on the pore size in this regime. Furthermore the existing prediction by Hall[22] in eq 1 is found to grossly underestimate the conductance for small concentrations, although entrance effects are allegedly taken into account to obtain this expression.

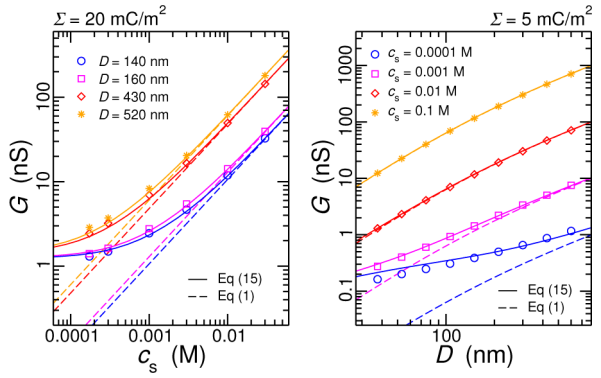

Figure 4. Pore conductance versus (a) salt concentration for $\Sigma = 20$ mC/m^2 and various pore diameters; (b) pore diameter for $\Sigma = 5$ mC/m^2 and various salt concentrations. Dashed lines are predictions using eq 1, while solid lines are predictions of the spatially extended surface conduction model, eq 15. In this equation, $\alpha = 2$ as proposed by Hall[22] and β is fixed to $\beta = 2$ so as to obtain the best agreement.

Going further, it is interesting to plot the contour lines of the electric potential for this geometry. Figure 5 compares the

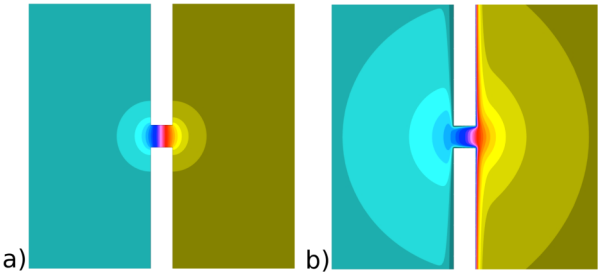

Figure 5. Contour lines of the electric potential across a typical pore ($L = D = 100$ nm) (a) without surface charge and (b) with surface charge (Dukhin length $l_{Du} \sim 3D$).

electric map without (a) and with (b) a surface charge inside the pore. This shows that the surface charge perturbs the electric field and the corresponding electric current streamlines deeply outside the pore, well into the bulk of the reservoirs. The typical extension of this perturbation is given by the Dukhin length l_{Du} introduced above. This highlights that entrance effects should account for this perturbation in order to rationalize the numerical and experimental results. We anticipate that a model of the transport, discussed below and taking into account this effect, is able to reproduce the numerical results obtained in Figure 4.

Theoretical Model: Access Effects Revisited. We now present a model describing these results. Because of the 3D geometry of the nanopore, it is not possible to obtain an exact analytical solution for the conductance. However, it is possible to develop an approximate model, which captures the main mechanism associated with the field lines perturbation outside the pore due to surface conduction effect inside the pore.

A missing point in the previous analysis is that the surface conduction induces a strong perturbation of the electric field lines and corresponding electric current streamlines outside the nanopore as highlighted in Figure 5, over an extension given by the Dukhin length l_{Du}. Surface transport of ions requires that current and ions should be supplied within the diffuse interface to obey charge conservation, thus bending the electric streamlines toward the pore surface. This mechanism was

dx.doi.org/10.1021/nl301412b | Nano Lett. 2012, 12, 4037–4044

pointed out by Khair and Squires in a simple semi-infinite geometry with a step change in the surface conductance[15] and is highlighted in writing the condition for conservation of electric current at the surface of the pore. This imposes the following condition on the normal and tangential electric field[15]

$$\kappa_b E_n = \frac{\partial}{\partial z}[\kappa_s \Theta(z) E_z] \tag{7}$$

at the surface of the pore ($r = D/2$); n is the normal to the pore surface and z is the coordinate along the pore length; $\Theta(z)$ is the Heaviside step function along the length of the pore ($\Theta(z) = 0$ for $z < 0$, $z > L$ and $\Theta(z) = 1$ for $0 < z < L$). Note that this boundary condition (BC) introduces naturally the Dukhin length as a spatial variation for the field in the z direction. This BC complements the bulk transport equation, $\nabla \cdot \boldsymbol{E} = 0$, which follows from current conservation ($\boldsymbol{j} = \kappa_b \boldsymbol{E}$ and $\nabla \cdot \boldsymbol{j} = 0$). Unfortunately, these equations cannot be solved analytically, even for a simple planar situation as considered by Khair and Squires.[15]

However, some scaling estimate can be extracted, providing the leading behavior. For simplicity, we now focus on one side of the pore and will add up the two sides in the end. A difficulty encountered with the above equation lies in the step discontinuity of the surface conduction at the entrance, which thus acts as a current sink. However, this is the source of the coupling between bulk and surface transport. Indeed the above BC at the surface of the pore, eq 7, can be rewritten as

$$\kappa_b E_n = \kappa_s \delta(z) E_z + \kappa_s \Theta(z) \frac{\partial}{\partial z} E_z \tag{8}$$

for $r = D/2$ with $\delta(z)$ the Dirac distribution.

Now we consider an iterative solution to the equations for the electric field. In the previous parts above, one has neglected this effect and we denote as $E^{(0)}$ the corresponding solution for the electric field, including the access effects discussed by Hall and others.[21,22,25] We write accordingly the electric field as $E = E^{(0)} + \delta E$. Now, keeping only the most singular part of the BC on the electric field, the above BC for δE is to lowest order

$$\delta E_n \simeq l_{Du} E_z^{(0)} \delta(z) \tag{9}$$

for $r = D/2$, $z = 0$, and complementing the bulk equation $\nabla \cdot \delta \boldsymbol{E} = 0$. This corresponds to the electric field created by an annulus located as $z = 0$, with radius $r = D/2$ (at the mouth of the pore), with a line charge

$$\lambda_{an} = l_{Du} E_z^{(0)} \quad \left(r = \frac{D}{2}, \quad z = 0\right) \tag{10}$$

(normalizing the fictitious dielectric constant to unity, for simplicity). The solution for δE can then be written as

$$\delta \boldsymbol{E}(r) = \int \mathrm{d}\boldsymbol{r}' \lambda_{an} \delta(z') \delta\left(r' - \frac{D}{2}\right) \frac{\boldsymbol{r} - \boldsymbol{r}'}{4\pi |\boldsymbol{r} - \boldsymbol{r}'|^3} \tag{11}$$

The corresponding supplementary contribution to the electric current writes in the bulk

$$\delta I = \int d\boldsymbol{S} \kappa_b \delta \boldsymbol{E}(r) \sim \kappa_b Q \tag{12}$$

with $Q = 2\pi D \lambda_{an}$ the total charge of the annulus.

At this stage, we will leave the formal solution and extract the main scaling behaviors. According to the considerations by Hille[21] and Hall,[22] the typical electric field $E_z^{(0)}$ at the entrance is fixed by the voltage drop outside the pore, ΔV_{out}, over a distance given by the diameter of the pore. Accordingly, one has $E_z^{(0)}(r = (D/2), z = 0) \sim \Delta V_{out}/D$ and the total charge of the annulus writes $Q \sim l_{Du} \Delta V_{out}$ (reminding that the fictitious dielectric constant is set to unity).

Gathering the above results, one can deduce the supplementary contribution to the electric current as

$$\delta I \sim \kappa_b l_{Du} \Delta V_{out} \sim \kappa_s \Delta V_{out} \tag{13}$$

We write this result as $\delta I = \beta \kappa_s \Delta V_{out}$ with β as a numerical constant.

This is a quite counterintuitive result, showing that surface conductance effects do alter the electric current outside the nanopore, deep in the bulk, as pointed out by eq 11. It is however in direct agreement with the qualitative picture by Khair and Squires[15] and with Figure 5, which shows that surface conduction effects within the pore do extend spatially outside the pore over a "healing length" given by the Dukhin length l_{Du}.

From the above analysis, one may add up the various contributions to the electric current in the bulk as $I = I^{(0)} + \delta I$, giving

$$I = \alpha \kappa_b D \Delta V_{out} + \beta \kappa_s \Delta V_{out} \tag{14}$$

thus showing that the access conductance outside the pore depends directly on the surface conductance inside the pore: $G_{out} = \alpha \kappa_b D + \beta \kappa_s$. After some straightforward manipulations, the expression for the global conductance of the nanopore is then found as

$$G = \kappa_b \left[\frac{4L}{\pi D^2} \times \frac{1}{1 + 4\frac{l_{Du}}{D}} + \frac{2}{\alpha D + \beta l_{Du}} \right]^{-1} \tag{15}$$

where we recall that $l_{Du} = \kappa_s/\kappa_b$ is the Dukhin length. This equation is one of the main results of this paper. Interestingly, comparing eqs 15 and 4, the above result can be reinterpreted in terms of an increased apparent electric pore size, given by $D_{app} = D + \beta^\star l_{Du}$ (with $\beta^\star = \beta/\alpha$). The latter originates in the access conductance oustide the pore, G_{out}, which can be rewritten as $G_{out} = \alpha \kappa_b D_{app}$, which is in line with Hille and Hall result,[21,22] but with the bare size replaced by the apparent electric size D_{app}. Some limiting behavior of the above results are also interesting to discuss. In the limit of large Dukhin lengths $l_{Du} \gg D$, which occurs for low salt concentration, $c_s \to 0$, and/or large surface charge $|\Sigma|$, the conductance behaves as

$$G(l_{Du} \to \infty) = \kappa_s \left(\frac{4L}{\pi D} + \frac{2}{\beta} \right)^{-1} \tag{16}$$

Therefore the present mechanism indeed predicts a saturation of the conductance for small concentration, which stems from the fact that $D_{app} \gg D$ in this limit. Furthermore the conductance in this limit is shown to depend only on the aspect ratio L/D of the pore, but not explicitly on the diameter D. In a counterintuitive way, small pores can conduct as efficiently as large pores!

Comparison with Numerical Results. We have compared the above predictions with the results of the full numerical calculations described above. Equation 15 is plotted in Figure 4 against the numerical results. We note that in this plot the surface conductance is calculated independently as a function of the surface charge, using theoretical expression of the nonlinear Poisson−Boltzmann framework (see ref 18 and Methods) and is not a free parameter. We fixed $\alpha = 2$ as suggested by Hall[22]

dx.doi.org/10.1021/nl301412b | Nano Lett. 2012, 12, 4037−4044

and Kowalczyk et al.;[25] The only remaining free parameter, β, was tuned to $\beta = 2$ in order to obtain the best match. Therefore, the full numerical calculations indicate that $\beta^{\star} = \beta/\alpha = 1$. Consequently, the apparent electric pore size simplifies to $D_{app} \simeq D + l_{Du}$. Overall the prediction of eq 15 yields an excellent match with the results of the numerical calculations, thus demonstrating that the above approach does capture the physical mechanism at play.

Of course, the previous model contains some simplification for charge transport, leaving aside, for example, the detailed single ion chemical equilibrium and concentration polarization. However, these effects are included in the full numerical description, and it is therefore quite remarkable that the simple electric conduction model above is able to reproduce quantitatively numerical results for ion transport.

Comparison with Experimental Results. Having now a physically relevant picture for the electric conduction in a nanopore, we can come back to the experimental results (presented in Figure 2). In Figure 6, the measured conductance

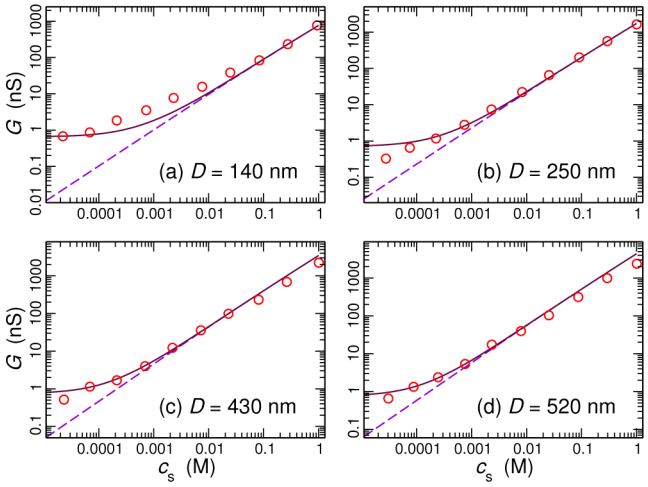

Figure 6. Comparison between the measured conductance and the predictions by eq 1 (dashed line) and eq 15 (solid line), in nanopores with different diameters of (a) 140, (b) 250, (c) 430, and (d) 520 nm. The only free parameter to fit all experimental data is the surface conductance, which was fixed to $\kappa_s = 0.8$ nS to obtain best agreement (corresponding to a surface charge $|\Sigma| \approx 11$ mC/m^2) . A good agreement between the measured conductance and predicted value is observed.

is compared with eq 15. We used $\alpha = \beta = 2$, as previously determined by numerical calculations, and the bulk conductivity κ_b measured independently. The only remaining free parameter, κ_s, was tuned to $\kappa_s = 0.8$ nS to obtain best agreement. Using the approximate expression $l_{Du} = \kappa_s/\kappa_b \approx (|\Sigma|/e)/(2c_s)$ (see Methods), this corresponds to a surface charge $|\Sigma| \approx 11$ mC/m^2, compatible with previous experimental values.[29,30]

As seen in Figure 6, several key features observed in the experimental results such as a transition from bulk conductance dominated regime to surface conductance dominated regime and a saturation of the conductance at low salt concentration are well predicted by eq 15. Overall, the agreement between the predicted value and experimental results is good. A slight deviation at intermediate salt concentrations is observed for 140 nm diameter, which might be attributed to a conical shape observed in 140 nm diameter pore. The change in the conductance as a function of pore diameter is shown in Figure 7 along with the prediction by eqs 1 and 15. For a high salt

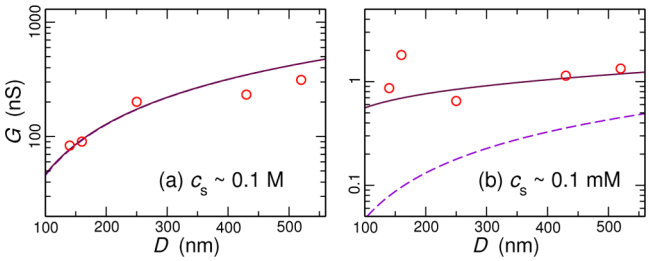

Figure 7. Conductance versus pore diameter at salt concentration of (a) ~0.1 M and (b) ~0.1 mM (exact values were deduced from bulk conductivity measurements). The dashed line is the predicted conductance by eq 1, while the solid line is the predicted conductance by eq 15. Values of the parameters are identical to Figure 6.

concentration of 0.1 M KCl, the experimental data are in excellent agreement with the predictions by both equations, confirming the dominance of bulk conduction at this salt concentration. But for a low salt concentration of 0.1 mM only eq 15, which takes into account both surface conductance and access effect, exhibits good agreement with the experimental data. Furthermore the conductance depends weakly on the pore size and is roughly 1 order of magnitude larger than what predicted if one ignores surface conduction contribution to the access effect.

Conclusions. In conclusion, we have shown that the transport of ions in solid-state nanopores exhibit complex features, which strongly depart from what is observed in nanochannels. The three-dimensional nature of the system couples to the surface conduction inside the nanopore to induce unexpected electrical access effects that cannot be neglected. This is shown to lead to an anomalously large ion conductance at small ion concentration and/or large surface charge. We developed a simplified analytical model for the conduction in nanopores, which provides a very good agreement with both numerical calculations of the full transport equations and with experimental results. This supports the idea that ion transport is strongly perturbed outside the pore over a healing length given by the so-called Dukhin length, $l_{Du} = \kappa_s/\kappa_b$ the surface to bulk conductivity ratio, in order to meet ion current conservation at the entrance of the nanopore.[15] Altogether the results can be interpreted in terms of an apparent electric diameter D_{app} of the nanopore, which is the sum of the bare geometric size of the pore and the Dukhin length

$$D_{app} = D + l_{Du} \tag{17}$$

(using $\alpha = \beta$ as obtained numerically). This apparent size of the pore is thus controlled by electric entrance effects whenever the Dukhin length l_{Du} is large compared to the bare geometric size of the nanopore. This is quantified by the Dukhin number, Du $= 4l_{Du}/D$, which, on top of geometric scale D of the nanopore, involves physicochemical parameters such as the surface conductivity/surface charge of the pore. As a simple rule of thumb, this Dukhin number can be interpreted as the ratio between the number of surface charges on the nanopore surface to the number of bulk charges that it contains; Du $\sim N_{surface}/N_{bulk}$ with $N_{surface} = (|\Sigma|/e)(\pi DL)$ and $N_{bulk} = 2c_s(\pi/4)D^2L$, where Σ is the surface charge density, and we used the Poisson−Boltzmann estimate for the surface conductivity (see

dx.doi.org/10.1021/nl301412b | Nano Lett. 2012, 12, 4037−4044

ref 18 and Methods). This clearly points to a surface to volume balance. Accordingly the entrance effects reported here will lead to anomalously large ion transport whenever surface charge dominate over the bulk ones (large Dukhin number). As highlighted in eq 16, the conductance in this regime only depends on the aspect ratio of the nanopore, but not directly on the bare geometric diameter D; for a fixed aspect ratio, small pores conduct as efficiently as large pores!

Such a situation of large Dukhin number will occur for highly charged and very small nanopores, which is the case of most biological transmembrane systems, even for relatively large salt concentration. For example, considering the alpha-hemolysin proteinic channel, at neutral pH and for isotonic conditions (e.g., 150 mM NaCl), the number of surface charges can be estimated to be twice as large as the number of bulk ones in the channel,[31] so that the Dukhin number is substantially larger than one (Du $\sim$ 2). Accordingly, entrance effects are expected to play a central role in the ionic transport through this channel, as accounted for by our prediction in eq 15. Furthermore, the electric entrance effects should be also taken into account when interpreting quantitatively translocation experiments of nanoparticles and molecules through solid-state or biological nanopores. Indeed our result show that the global conductivity of the pore involves information over a region which extends on a size D_{app}, which can be much larger than the bare geometric size of the pore. Consequently, the sensitivity to translocation events, which is usually measured via ion current variations as discussed in the introduction, should therefore integrate the corresponding information outside the pore. In particular, one expects that charged molecules or nanoparticles will follow the perturbed electric field lines at the entrance of the pore. Their influence is accordingly expected to be monitored far beyond the pore entrance, thus limiting the spatial resolution of such a technique. This is particularly relevant in view of the recent efforts to use ultimately thin nanopore devices such as pierced graphene sheets.[28,32]

Methods. *Nanopore Fabrication and Experiments.* Nanopores are fabricated on silicon nitride (SiN) membranes purchased from Silson Ltd. (Northampton). The microchip consists in a rectangular silicon nitride membrane (40 μm × 40 μm) in a square silicon supporting frame (7.5 mm × 7.5 mm). The thickness of the membrane is set to 100 nm.

A dual-beam column (ZEISS-GEMINI), Focused Ion Beam (FIB)/Scanning Electron Microscope (SEM), for the micro drilling of the silicon nitride membrane is used. FIB columns are able to focus highly energetic ions (typically GaC) to small spot sizes on the order of 5−20 nm. The interaction between energetic ions and the silicon nitride membrane results in localized material removal due to ion sputtering interactions. The membrane is placed at a position where both electron and ion columns can simultaneously image the same region of the sample, which greatly simplifies the location of the hole drilled by the FIB. Standard parameters for hole drilling are: 1 pA for the ion beam current with a FIB columns voltage set to 35 keV. Time of drilling is accordingly modified to obtain nanopores with different diameters (140, 160, 250, 430, and 520 nm).

The image of transmission electron microscopy (TEM-TOPCON002B) is employed to determine diameter and shape of each nanopore as shown in Figure 1c. The pores with a large diameter (250, 430, and 520 nm) has a cylindrical shape, but nanopores with a diameter of 140 and 160 nm are slightly conical (±10 nm in diameter).

Conductance Measurements. To measure ion conductance in a single nanopore, a flow cell is built with polyether ether ketone (PEEK), and the SiN membrane with a nanopore is inserted between two half-cells and sealed with O-ring (Figure 1). Before the membrane is placed into a flow cell, the latter is cleaned with acetone, isopropanol, and deionized water for 10 min each. Potassium chloride (KCl) solutions (pH 6) with varying concentration are prepared by serial dilution of 1 M KCl solution with deionized water (18.2 MΩ·cm, Millipore). The bulk conductivity of prepared KCl solutions is measured with conductivity meter (CHI 2300, HANNA Instruments) right before the conductance measurement with a nanopore. Test liquids are degassed before each measurement to prevent any nucleation of nanobubbles inside a pore. During the measurement, a transmembrane voltage between −0.1 to 0.1 V is applied with 0.01 V step using Ag/AgCl electrodes immersed in each half-cell. The resulting electrical current through the membrane is measured with the same Ag/AgCl electrodes connected to the amplifier at an acquisition rate of 10 kHz using LabView program. Conductance is calculated by linearly fitting voltage-current curve.

The experimental data for the measured conductance over a wide range of salt concentrations in each nanopore are shown in Figure 2 of the main text, while the representative voltage-current curve for 140 nm diameter nanopore is shown in the corresponding inset. In all nanopores studied, voltage−current curve exhibits a linear relationship in the transmembrane voltage range between −0.1 and 0.1 V. Conductance measurements performed for different pH value do not show significant variations.

Poisson−Boltzmann Calculation of the Surface Conductivity. In order to compare the theoretical prediction eq 15 with the numerical results, one has to compute the surface conductivity κ_s, or equivalently the Dukhin length $l_{Du} = \kappa_s/\kappa_b$, as a function of surface charge Σ, salt concentration c_s and pore diameter D. Within the Poisson−Nernst−Planck framework, the electric current I_e through a charged cylindrical channel can be written as the integral of the electric flux over the channel cross section

$$\frac{I_e}{E_z} = e^2\mu \int_S (c_+ + c_-)\mathrm{d}S \tag{18}$$

where E_z is the electric field applied along the tube axis and other quantities have been defined in the main text. This current can be decomposed as the sum of bulk and surface contributions

$$\frac{I_e}{E_z} = \frac{\pi D^2}{4}\kappa_b + \pi D\kappa_s = \frac{\pi D^2}{4}\kappa_b\left(1 + \frac{4l_{Du}}{D}\right) \tag{19}$$

In the absence of surface charge, $c_+ = c_- = c_s$ everywhere. Using eqs 18 and 19 with $\kappa_s = 0$, one immediately gets $\kappa_b = 2e^2\mu c_s$. The Dukhin length can then be computed as

$$l_{Du} = \frac{D}{4}\left\{\frac{2}{\pi D^2 c_s}\int_S (c_+ + c_-)\mathrm{d}S - 1\right\} \tag{20}$$

The ion density profiles inside the channel were computed assuming a Boltzmann distribution, $c_\pm = c_s e^{\mp eV/k_BT}$, after we solved numerically the nonlinear Poisson−Boltzmann (PB) equation for the electric potential V

dx.doi.org/10.1021/nl301412b | Nano Lett. 2012, 12, 4037−4044

$$\Delta V = \frac{2ec_s}{\varepsilon}\sinh\left(\frac{eV}{k_BT}\right) \tag{21}$$

Going further, it is possible to derive an approximate expression for the Dukhin length under the assumption that the EDL width is small as compared to the channel diameter, so that the potential is similar to the one near a plane wall in a semi-infinite solution. Therefore, we will use the nonlinear PB solution in this situation, considering that the potential vanishes at infinity. Consequently, the potential reads

$$V(x) = -2\frac{k_BT}{e}\log\left(\frac{1+\gamma\exp\left(\frac{-x}{\lambda_D}\right)}{1-\gamma\exp\left(\frac{-x}{\lambda_D}\right)}\right) \tag{22}$$

where x is the distance to the wall, and γ is given by

$$\gamma = -\frac{l_{GC}}{\lambda_D} + \sqrt{\frac{l_{GC}^2}{\lambda_D^2}+1} \tag{23}$$

with the Gouy–Chapmann length $l_{GC} = 2\varepsilon k_BT/(|\Sigma|e)$ (see ref 18). Using eq 20 and this expression for the electric potential, the Dukhin length can be computed as

$$l_{Du} = \frac{|\Sigma|/e}{2c_s}\gamma \tag{24}$$

with γ given in eq 23. For typical experimental surface charges with $|\Sigma| \sim 10$ mC/m^2, this approximate expression matches almost perfectly the exact numerical values (<1% error). This can be understood since, in this regime of large surface charge, most of the EDL charge is contained in the Gouy–Chapmann region of width $l_{GC} \sim 4$ nm $\ll D$. The wall curvature and EDL overlap can therefore be neglected. As a matter of fact, for low salt concentrations, where the effect of surface conduction becomes significant, one has $l_{GC} \ll \lambda_D$, and $\gamma \approx 1$. Consequently, the even simpler expression $l_{Du} = (|\Sigma|/e)/(2c_s)$ is perfectly suited to fit the experimental data.

AUTHOR INFORMATION

Corresponding Author

*E-mail: lyderic.bocquet@univ-lyon1.fr

Notes

The authors declare no competing financial interest.

ACKNOWLEDGMENTS

We thank N. Blanchard for help with the FIB and D. Guillot for building the fluidic cell. We acknowledge support from ERC, AG-project *Micromega*.

REFERENCES

(1) Napoli, M. T.; Pennathur, S.; Eijkel, J. C. T. *Lab Chip* **2010**, *10*, 957–985.
(2) Howorka, S.; Siwy, Z. *Chem. Rev. Lett.* **2009**, *38*, 2360–2384.
(3) Siwy, Z. S.; Howorka, S. *Chem. Rev. Lett.* **2010**, *39*, 1115–1132.
(4) Striemer, C. C.; Gaborski, T. R.; McGrath, J. L.; Fauchet, P. M. *Nature* **2007**, *445*, 749–753.
(5) Vlassiouk, I.; Apel, P. Y.; Dmitriev, S. N.; Healy, K.; Siwy, Z. S. *Proc. Natl. Acad. Sci. U.S.A.* **2009**, *106*, 21039–21044.
(6) Humplik, T.; et al. *Nanotechnology* **2011**, *22*, 292001.
(7) Guo, W.; et al. *Adv. Funct. Mater.* **2010**, *20*, 1339–1344.
(8) Saleh, O. A.; Sohn, L. L. *Proc. Natl. Acad. Sci. U.S.A.* **2003**, *100* (3), 820–824.
(9) Dekker, C. *Nat. Nanotechnol.* **2007**, *2*, 209–215.
(10) Sexton, L. T.; Mukaibo, H.; Katira, P.; Hess, H.; Sherrill, S. A.; Horne, L. P.; Martin, C. R. *J. Am. Chem. Soc.* **2010**, *132*, 6755–6763.
(11) Uram, J. D.; Ke, K.; Hunt, A. J.; Mayer, M. *Small* **2006**, *2*, 967–972.
(12) Branton, D.; et al. *Nat. Biotechnol.* **2008**, *26* (10), 1146–1153.
(13) Carbonaro, A; Sohn, L. L. A. *Lab Chip* **2005**, *5*, 1155–1160.
(14) Kalman, E. B.; Sudre, O.; Vlassiouk, I.; Siwy, Z. S. *Anal. Bioanal. Chem.* **2009**, *394*, 413–419.
(15) Khair, A. S.; Squires, T. M. *J. Fluid Mech.* **2008**, *615*, 323–334.
(16) Stein, D.; Kruithof, M.; Dekker, C. *Phys. Rev. Lett.* **2004**, *93* (3), 035901.
(17) Schoch, R. B.; van Lintel, H.; Renaud, P. *Phys. Fluids* **2005**, *17*, 100604.
(18) Bocquet, L.; Charlaix, E. *Chem. Soc. Rev.* **2010**, *39*, 1073–1095.
(19) Ho, C.; Qiao, R.; Heng, J. B.; Chatterjee, A.; Timp, R. J.; Aluru, N. R.; Timp, G. *Proc. Natl. Acad. Sci. U.S.A.* **2005**, *102*, 10445–10450.
(20) Smeets, R. M. M.; Keyser, U. F.; Krapf, D.; Wu, M.-Y.; Dekker, N. H.; Dekker, C. *Nano Lett.* **2006**, *6* (1), 89–95.
(21) Hille, B. *J. Gen. Physiol.* **1968**, *51*, 199219.
(22) Hall, J. E. *J. Gen. Physiol.* **1975**, *66*, 531–532.
(23) Willmott, G. R.; Smith, B. B. *Nanotechnology* **2012**, *23*, 088001.
(24) Vodyanoy, I.; Bezrukov, S. M. *Biophys. J.* **1992**, *62*, 10–11.
(25) Kowalczyk, S. W.; Grosberg, A. Y.; Rabin, Y.; Dekker, C. *Nanotechnology* **2011**, *22*, 315101.
(26) Wanunu, M.; Dadosh, T.; Ray, V.; Jin, J.; McReynolds, L.; Drndic, M. *Nat. Nanotechnol.* **2010**, *5*, 807–814.
(27) Garaj, S.; Hubbard, W.; Reina, A.; Kong, J.; Branton, D.; Golovchenko, J. A. *Nature* **2010**, *467*, 190–193.
(28) Schneider, G. F.; et al. *Nano Lett.* **2010**, *10*, 3163–3167.
(29) Sonnefeld, J. *Colloid Surf. A* **1996**, *108*, 2731.
(30) Cerovic, L. S.; Milonjic, S. K.; Bahloul-Hourlier, D.; Doucey, B. *Colloid Surf. A* **2002**, *197*, 147156.
(31) Song, L.; Hobaugh, M. R.; Shustak, C.; Cheley, S.; Bayley, H.; Gouaux, J. E. *Science* **1996**, *274*, 1859.
(32) Merchant, C. A.; Healy, K.; Wanunu, M.; Ray, V.; Peterman, N.; Bartel, J.; Fischbein, M. D.; Venta, K.; Luo, Z.; Johnson, A. T. C.; Drndic, M. *Nano Lett.* **2010**, *10*, 2915–2921.